Arabian Journal of Geosciences (2019) 12: 475
https://doi.org/10.1007/s12517-019-4601-z

ORIGINAL PAPER

Geochemical characteristics of the karst-type bauxites: an example from the Kanirash deposit, NW Iran

Ali Abedini[1] · Masoud Habibi Mehr[1] · Maryam Khosravi[2] · Ali Asghar Calagari[3]

Received: 8 January 2019 / Accepted: 2 July 2019 / Published online: 29 July 2019

Abstract

The Kanirash bauxite deposit belongs to the Iran-Himalayan karst-type bauxite belt, which is situated about 30 km southeast of Mahabad city, northwestern Iran. The bauxite ores are embedded by the Late Permian carbonate rocks intercalated with shale of the Ruteh Formation and occurred as layer and lens-shaped patches. The bauxite ores contain diaspore, clinochlore, hematite, pyrophyllite, illite, rutile, and lesser amounts of zircon, pyrite, and barite. This mineral assemblage indicates that this deposit was formed in a transitional zone between the vadose and the phreatic environments. The presence of pyrite in the bauxite ores demonstrates that organic matters were present in the uppermost parts of the profile and the depositional diagenetic/epigenetic environment was reducing. Ti and Fe together with a suite of trace elements, including Ni, Cr, Co, Ga, Ta, and V, were leached from the upper parts of the weathered profile and concentrated in the bottom parts with respect to Hf, chosen as the least mobile element. Some factors, such as pH variations in weathering solutions, buffering nature of the carbonate bedrock, mineral control, the existence of organic materials, and fluctuations of groundwater table played important roles in distribution of trace and rare earth elements.

Keywords Kanirash bauxite deposit · Mass change · Fluctuations of groundwater level · Iran

Introduction

Bauxite, though generally exploited as an Al ore, is also a major source of several trace elements, notably the high field strength elements (HFSEs) Ti, Nb, P, and Zr, as well as Ni, Au, Ga, Co, V, Cr, and rare earth elements (REEs). These elements may be hosted by authigenic as well as detrital minerals, such as zircon, tourmaline, and rutile (Liu et al. 2010; Wang et al. 2010, 2012; Gamaletsos et al. 2017; Abedini and Calagari 2014; Ling et al. 2013, 2015, 2017, 2018), which are stable in the supergene environment (Nesbitt 1979; Gamaletsos et al. 2017). Bauxites are the weathered deposits that are developed from intense chemical weathering of aluminosilicate-rich parent rocks under humid, tropical to subtropical climate conditions (Bárdossy 1982) and are restricted to a belt between 30° north latitude and 30° south latitude (Tardy et al. 1991). In turn, bauxitization is a result of a good drainage under humid, tropical climate and moderate relief (Marker and Oliveira 1994). The formation of bauxite is controlled by the geographic latitude, atmospheric climate, and special climatic periods (e.g., the amount of CO_2 in the Earth's atmosphere or greenhouse effect) (Bárdossy and Aleva 1990; Gamaletsos et al. 2017) that are accompanied with intense weathering during limited time intervals (Bárdossy and Aleva 1990; Gamaletsos et al. 2017). Based upon the bedrock lithology, bauxites were categorized into karst- and laterite-type bauxites (Bárdossy and Aleva 1990). The laterite-type bauxites lied on aluminosilicate rocks and are mainly autochthonous, whereas the karst-type bauxites are rested on carbonate rocks being either autochthonous or allochthonous in origin. Geochemical and mineralogical composition of bauxites provides some enlightenments on drainage conditions controlled by climatic signatures and morphological conditions (Marker and Oliveira 1994). Thus, geochemical and mineralogical interpretations

Editorial handling: Maurizio Barbieri

✉ Ali Abedini
abedini2020@yahoo.com; a.abedini@urmia.ac.ir

[1] Department of Geology, Faculty of Sciences, Urmia University, Urmia 5756151818, Iran

[2] Department of Earth Sciences, Faculty of Sciences, Shiraz University, Shiraz 7146713565, Iran

[3] Department of Earth Sciences, Faculty of Natural Sciences, University of Tabriz, Tabriz 5166616471, Iran

of the bauxite ores will furnish profound insights into reconstruction of the palaeo-climate conditions and effect of climate-driven changes in development of the bauxite profiles. Concentrations of the REE in the karstic bauxites are higher than those in the lateritic bauxites (Mameli et al. 2007; Karadag et al. 2009; Boni et al. 2013; Hanilçi 2013), suggesting that differences in the source lithology and/or weathering mechanism of different bauxites potentially play important roles in concentrating REE (Mongelli 1997; Mameli et al. 2007; Liu et al. 2010; Ling et al. 2018).

Depositional diagenetic/epigenetic environment of bauxites on the basis of hydrological, geochemical, and mineralogical studies was classified into vadose- and phreatic-type (Bárdossy 1982; D'Argenio and Mindszenty 1995; Ling et al. 2017). Mineralogically, the vadose-type bauxites, characterized by seasonal high groundwater table (SHGWT) under neutral and oxidizing conditions, include gibbsite, boehmite, hematite, and goethite (Bárdossy 1982; D'Argenio and Mindszenty 1995). On the contrary, the phreatic-type bauxites, including diaspore, boehmite, goethite, siderite, and pyrite mineral assemblage, represent seasonal low groundwater table (SLGWT) under acidic and reducing conditions (D'Argenio and Mindszenty 1995). The presence of sulfides (e.g., pyrite) in bauxites provides insights into the role of microorganisms in generation of bauxite profiles and the physicochemical conditions during the development of bauxite deposits.

The bauxite deposits in Iran are located in four structural zones: (1) Alborz Mountains, (2) the Zagros Simply Folded Belt, (3) the Sanandaj-Sirjan Metamorphic Zone, and (4) the Central Iran. They were temporally developed within a period ranging from Permian to Middle Cretaceous (Calagari and Abedini 2007; see Fig. 1a). However, the karst-type bauxite deposits of Iran are spatially limited to northwestern Iran. Most of the bauxite deposits of Iran are low-grade. The Jajarm deposit situated in the Alborz Mountains (see Fig. 1a) is the largest bauxite deposit in Iran that is currently mined as an open pit. Reserve of more than 19 Mt of bauxite ores with an average Al_2O_3/SiO_2 ratio of 43/14 for this deposit had been estimated (Esmaeily et al. 2010). No precise data for reserves and average grades of aluminum of the other bauxite deposits of Iran, especially of northwestern Iran, are available. Bauxite deposits of Permian and Permo-Triassic age have chiefly been reported from northwestern Iran. The effusion of volcanic rocks in the Alborz Mountains and northwestern Iran during the Late Permian was accompanied with an increase in CO_2 level locally in the Earth's atmosphere that brought about warm and humid climate and intensified bauxitization (Braun et al. 1998).

On the other hand, Iran in the Permian was located at zero degree latitude (cf. Muttoni et al. 2009) that facilitated weathering of the source rocks and generated the bauxite profiles. Additionally, high rainfall and temperature during the Late Permian (Muttoni et al. 2009, references therein) with favored chemical, physical, and biological weathering led to the development of the bauxite profiles in northwestern Iran. The objective of this paper is to gain a better understanding of the role of microorganisms and the underlying carbonate rocks together with climate changes and fluctuations of groundwater levels in the distribution of the REE and development of the bauxite ores at Kanirash. In other words, mineralogical and geochemical considerations were performed with the aim of understanding differential mobility and distribution of trace elements, especially of the REE, along the entire studied profile.

Geological setting and deposit geology

Bauxite deposits in Iran belong to the Iran-Himalayan karst-type bauxite belt and were generally developed in karstic sinkholes and depressions of the Mesozoic marine sedimentary carbonate rocks deposited in the Paleo-Tethys Ocean (e.g., Gamaletsos et al. 2017, and references therein). The Kanirash bauxite deposit is located in the Sanandaj-Sirjan Metamorphic Zone (see Fig. 1a). The bauxite deposits in northwestern Iran are distributed temporally from Permian to Jurassic (Abedini and Calagari 2013a). Epeirogenic movements during the Late Permian were accompanied by different cessations of shale and carbonate deposition of the Ruteh Formation in northwestern Iran, instead of the occurrence of basic volcanism in the Alborz Mountains in general and in some districts of northwestern Iran in particular (Kamineni and Efthekharnezad 1977; Abedini and Calagari 2013b). Following epeirogenic movements and uplift events, the bauxite profiles were developed within the carbonate rocks intercalated with shale of the Ruteh Formation. The mafic igneous rocks in northwestern Iran were regarded as a source rock for the bauxite ores. The patches of these mafic rocks in some districts of this region are sandwiched between the bauxite horizons and the underlying carbonate rocks (Abedini and Calagari 2013c, 2015, 2017, Abedini et al. 2019a, b; Khosravi et al. 2017).

The Kanirash bauxite deposit is situated about 30 km of southeastern Mahabad city (West-Azarbaidjan province), NW Iran (see Fig. 1b). The Precambrian Kahar Formation (phyllite, gneiss, and acidic volcanic rocks) is the oldest lithologic sequence in the study area (see Figs. 1b and 2). The Mahabad (volcanic rocks, shale, and limestone), Soltanieh (dolomite and shale), and Lalun (sandstone) Formations, in order of decreasing age, belong to Cambrian and are overlain by cherty dolomite and flaggy limestone of the Mila Formation (Cambro-Ordovician) and dolomitized limestone intercalated with shale of the Ruteh Formation (Late Permian; see Fig. 2). The bauxite ores at Kanirash overlie the carbonate rocks intercalated with shale of the late Permian Ruteh Formation. They occurred as stratified and

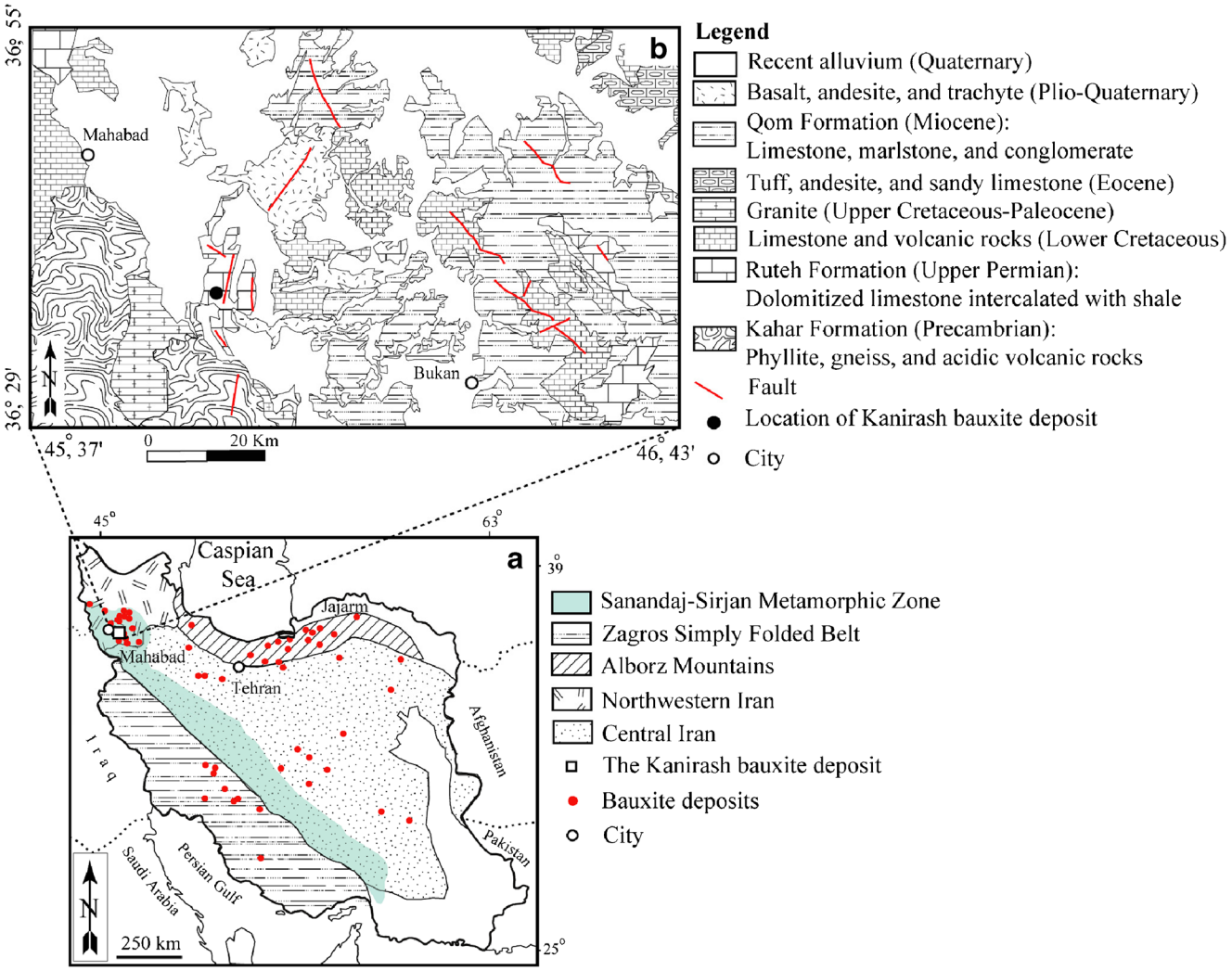

Fig. 1 **a** Spatial distribution of the bauxite deposits (shown by red dots) in map of Iran (from Khosravi et al. 2017) and position of the Kanirash bauxite deposit (marked by a quadrangle) within the Sanandaj-Sirjan Metamorphic Zone. **b** Simplified geological map showing situation of the Kanirash bauxite deposit in a regional scale

lenticular horizons with overall trends of NW-SE and N-S (see Fig. 2).

Method of investigation

A profile perpendicular to the trend of one of the bauxite profiles was selected for detailed mineralogical and geochemical studies (see Fig. 2). Sampling was carried out from the bauxite ores, the enclosing sedimentary rocks (shale and limestone of the Ruteh Formation), and the mafic volcanic rocks (basalt). The ores were sampled with 1-m intervals and on the basis of their physical aspects (chiefly color) classified into three distinct units, including dark green bauxite ore (DGBO) at the top, brownish red bauxite ore (BRBO) at the middle, and red bauxite ore (RBO) at the bottom of the selected profile (see Fig. 3). Samples from Bu-1 to Bu-3 are of the RBO unit, from Bu-4 to Bu-7 of the BRBO unit, and from Bu-8 to Bu-16 of the DGBO unit.

Microscopic examinations were done on 25 thin-polished sections of the bauxite ores with the aim of identifying the textural features of the ores. Eight representative samples of all the bauxite units (2 samples of the RBO unit, 2 samples of the BRBO unit, and 4 samples of the DGBO unit) were selected and ground in order to determine the major rock-forming minerals. Results of mineralogical composition of the bauxite ores are presented in Table 1. Mineralogical analyses were executed by Siemens D5000 X-Ray diffractometer at the Geological Survey of Iran under the following conditions: Cu-Kα radiation, 40 kV, 30 mA, scanning speed 8° per minute, and scan range 2°–60°. Microscopic mineral identification was carried out at the Geology Department of Urmia University, using Olympus BX60F5 optical microscope. Scanning electron microscopy (SEM) was performed by using

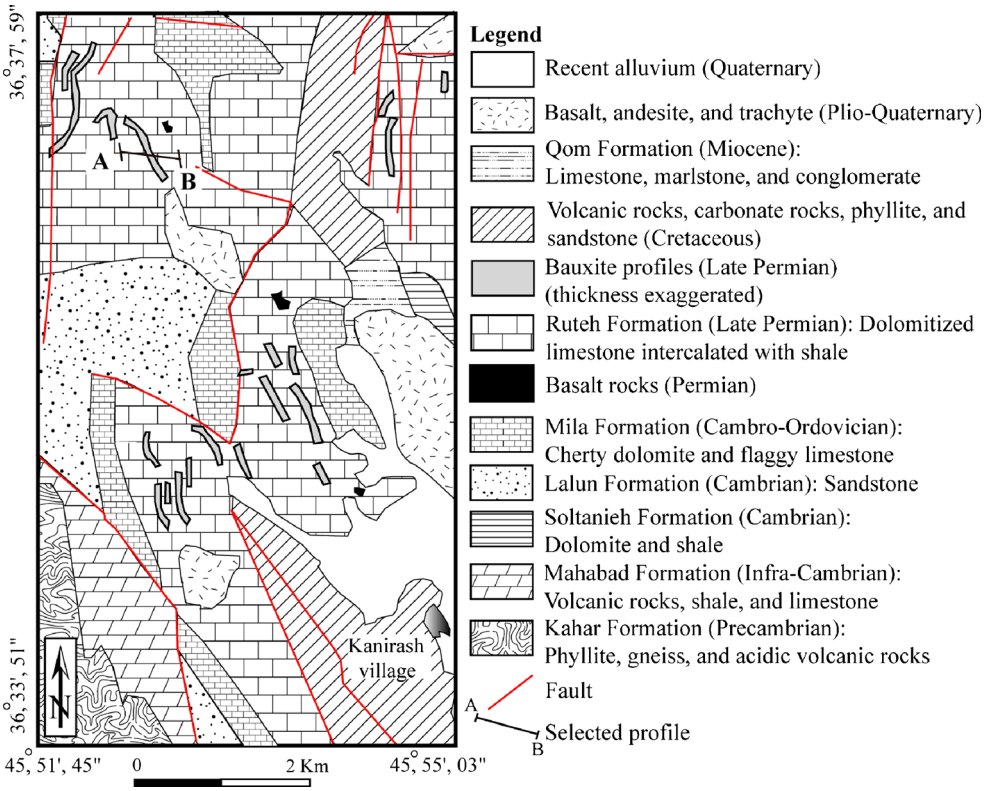

Fig. 2 Simplified and rather detailed geologic map of the study area showing the positions and trends of the bauxite horizons within the Late Permian Ruteh Formation (limestone with intercalated shale)

the TESCAN model VEGA II XMU in low vacuum equipped with a Link Analytical Oxford IE 350 energy-dispersive X-ray spectrometer (EDS). SEM-EDS analysis was conducted for four thin-polished sections at the Razi Metallurgical Research Center, Tehran under the following conditions: accelerating voltage of 15 kV, the beam current of 1 nA, and a beam diameter of 1 μm. Acquisition time was 70 s.

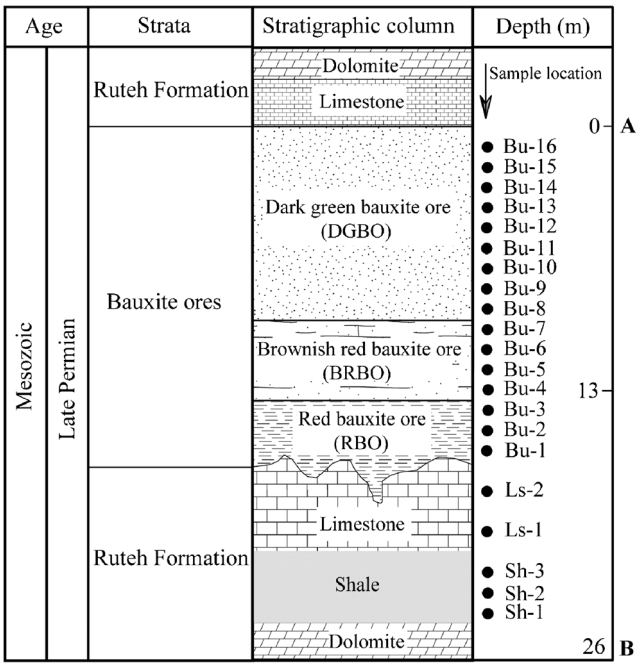

Fig. 3 Stratigraphic column along one of the bauxite profiles in the Kanirash bauxite deposit (refer to Fig. 2 for position and trend of the selected profile). Positions of the representative samples of the bauxite ores, limestone and shale of the Ruteh Formation for geochemical and mineralogical studies are marked with the filled circles

Samples were ground in a tungsten-carbide shatter box and dried at 60 °C. Contents of major and minor elements for twenty-four powder samples (#16 bauxite ores, #3 shales, #2 limestones, and #3 basalts) were determined by X-ray fluorescence (XRF) using a Philips Model 1480 spectrometer at the Geological Survey of Iran. Contents of trace elements (including REE) were measured by inductively coupled plasma mass spectrometry (ICP-MS) method at the Geological Survey of Iran following a mixture of lithium tetraborate-lithium metaborate fusion and dilute nitric digestion. Detection limit of major, minor, and trace elements (including REE) is listed in Table 2. The values of LOI (loss on ignition) were measured after overnight heating at 1000 °C. Analytical accuracy of major and trace elements is ± 0.5% and ± 2%, respectively.

The degree of elemental mobility has been evaluated by using an absolute weathering index (AWI). Hf content in the representative ore samples of the Kanirash bauxite is close to that in the Upper Continental Crust (UCC), which is taken into account as a source rock for the bauxite ores at Kanirash. In mass change calculations, Hf content in the bauxite ores was considered as a least mobile element relative to the others (e.g., Al, Ti, Zr, Nb, Ta, Th, and Sc) that have been regarded as invariant elements during weathering processes (see

Table 1 Results of powder X-ray diffraction for the representative ore samples of the Kanirash bauxite

Samples	Rock type	Major phases	Minor phases
Bu-1	Red bauxite ore	Hematite, diaspore, pyrophyllite	Rutile, clinochlore
Bu-3	Red bauxite ore	Hematite, diaspore, pyrophyllite	Clinochlore, illite, rutile
Bu-5	Brownish red bauxite ore	Hematite, diaspore	Rutile
Bu-7	Brownish red bauxite ore	Hematite, diaspore, pyrophyllite	Clinochlore, rutile
Bu-9	Dark green bauxite ore	Diaspore, clinochlore	Rutile, illite
Bu-11	Dark green bauxite ore	Diaspore, clinochlore	Rutile
Bu-14	Dark green bauxite ore	Diaspore, clinochlore	Illite, rutile
Bu-16	Dark green bauxite ore	Diaspore, clinochlore	Rutile

MacLean et al. 1997; Mongelli 1997; Lopez et al. 2005; Liu et al. 2010; Hanilçi 2013). The AWI method has been accounted as a valid proxy for element mobility in the weathered materials (Duzgoren-Aydin et al. 2002) and bauxites (Mameli et al. 2007; Mongelli et al. 2014). Percentage change of elements were calculated by $[(X/Hf)_{\text{bauxite ore}}/(X/Hf)_{UCC} - 1] \times 100$ in which X is the selected element.

Results

Mineralogy and petrography

Compared to the BRBO and RBO units, the DGBO unit displays the more textural diversity in the selected profile. According to the optical microscopic examinations, fluidal-collomorphic (Fig. 4a), cataclastic (Fig. 4b), and ooidic (Fig. 4c) textures are present in the DGBO unit, whereas the BRBO and RBO units are characterized by allothigenic clasts (Fig. 4e) and pisoids (Fig. 4f), respectively. Based upon results of mineralogical analyses, the bauxite ores contain diaspore, hematite, and clay minerals (e.g., pyrophyllite and clinochlore), which are the main rock-forming minerals (see Table 1 and Fig. 5) accompanied by minor phases like rutile and illite. Diaspore and clinochlore are the main constituents of the bauxite ores in the upper parts of the profile (DGBO unit), whereas hematite, diaspore, and pyrophyllite are the dominant constituent phases of the bauxite ores in the middle and basal parts (BRBO and RBO units; Table 1). Rutile occurs as a minor phase in the all of bauxite units. Based upon SEM-EDS observations, pyrite (Fig. 6a), barite (Fig. 6b), and zircon (Fig. 6c) were detected in the upper parts of the profile (DGBO unit), whereas diaspore and pyrophyllite (Fig. 6d) are present in the middle parts (BRBO unit).

Geochemistry

The chemical analyses of the major, minor, and trace elements (including REE) and the selected elemental ratios for twenty-four representative samples of the bauxite ores, limestone, shale, and basalt from the Kanirash bauxite deposit are presented in Tables 2 and 3, respectively. CaO (average 51 wt.%) is the main component in the limestone, whereas SiO_2 (average 63 wt.%) and Al_2O_3 (average 21 wt.%) are the main components in the shale of the Ruteh Formation. SiO_2, Al_2O_3, and Fe_2O_3 constitute about 80 wt.% of the whole chemical composition of the basalt. Al_2O_3 (32.6–50.3 wt.%), Fe_2O_3 (20.7–50 wt.%), SiO_2 (5.9–17.2 wt.%), and TiO_2 (3.3–7.2 wt.%) are the principal constituents (Table 2) and form more than 90 wt.% of the bauxite ores at Kanirash. Among the major elements, Fe_2O_3 and Al_2O_3 show the largest range of concentration.

Contents of the total REE (La-Lu) and the light REE (ΣLREE; La-Eu) in shale (average 193 ppm and 181 ppm, respectively) are higher than those in the basalt (average 107 ppm and 89 ppm, respectively) and the limestone (average 13 ppm and 12 ppm, respectively; Table 3). The heavy REE (ΣHREE; Gd-Lu) contents of the basalt (average 18 ppm), however, are higher than those of the shale and the limestone of the Ruteh Formation (average for both, 2 ppm). Contents of ΣLREE, ΣHREE, and ΣREE for the bauxite ores at Kanirash are 19.9–361.4 ppm (average 123 ppm), 6.8–33.7 ppm (average 13.1 ppm), and 26.7–383.9 ppm (average 136.5 ppm), respectively. The REE concentration normalized to C1 chondrite (values from Taylor and McLennan 1985) is indicated by the subscript N. The ratios of $(\Sigma LREE/\Sigma HREE)_N$ and $(La/Yb)_N$ in the bauxite ores are within the range of 1.5–9.6 (average 4.8) and 1.9–20.7 (average 7.8), respectively, which are not matched with those in the basalt, shale, and limestone (see Table 3). Values of the Eu anomaly observed in the basalt are close to unity (0.96–1.07) and those in the shale and limestone of the Ruteh Formation are about 0.6 (0.55–0.60 and 0.61–0.67, respectively; Table 3). Values of the Ce anomaly in the limestone are higher than those in the shale and the basalt in which the values are close to unity. Values of the Eu and Ce anomalies for sixteen representative ore samples of the Kanirash bauxite along the entire profile show ranges of 0.6–1.8 (with average of 0.9) and 0.9–3.1 (with average of 1.9), respectively.

Chondrite- and UCC-normalized REE spider diagrams are shown in Fig. 7. According to Fig. 7a, REE patterns for the three rock units in the selected profile are completely different from one another. The bauxite ores of the RBO (samples from Bu-1 to Bu-3) and BRBO (samples from Bu-4 to Bu-7) units are characterized by moderate fractionation of LREE from HREE with

Table 2 Results of whole rock chemical analyses of major, minor, and trace elements for 16 representative bauxite ores, 3 basalt, 3 shale, and 2 limestone samples in the Kanirash deposit

Samples	DL	Bu-1	Bu-2	Bu-3	Bu-4	Bu-5	Bu-6	Bu-7	Bu-8	Bu-9	Bu-10	Bu-11	Bu-12	Bu-13	Bu-14	Bu-15	Bu-16	Ls-1	Ls-2	B-1	B-2	B-3	Sh-1	Sh-2	Sh-3
Unit		RBO	RBO	RBO	BRBO	BRBO	BRBO	BRBO	DGCO	DGCO	DGCO	DGCO	DGCO	DGCO	DGCO	DGCO	DGCO	–	–	–	–	–	–	–	–
SiO_2 (wt.%)	0.01	5.87	7.34	6.13	10.68	6.72	16.03	17.23	12.26	13.16	12.62	13.55	14.86	14.72	11.14	11.72	12.56	2.66	8.36	51.98	52.77	52.81	63.34	64.02	62.03
TiO_2	0.01	3.32	3.51	3.66	3.56	3.77	3.45	3.45	5.21	4.62	3.96	3.98	5.25	4.34	7.21	4.76	4.77	0.03	0.03	2.97	2.87	3.03	0.97	0.92	0.97
Al_2O_3	0.01	32.63	34.26	39.15	37.89	43.78	37.65	38.96	45.03	43.01	44.51	42.36	39.22	40.11	46.32	50.32	42.95	0.91	0.46	13.32	13.62	13.54	21.24	20.11	22.16
Fe_2O_3	0.01	50.03	45.86	40.26	38.66	34.01	34.56	30.29	26.11	28.06	27.26	28.66	29.29	28.63	23.09	20.68	29.89	0.35	0.85	13.74	12.55	11.87	2.71	3.36	2.75
CaO	0.01	0.18	0.12	0.15	0.17	0.35	0.11	0.11	0.15	0.11	0.16	0.16	0.10	0.48	0.26	0.09	0.17	52.43	49.49	7.86	8.62	4.79	0.25	0.24	0.36
Na_2O	0.01	0.02	0.01	0.02	0.06	0.02	0.06	0.02	0.01	0.01	0.01	0.01	0.01	0.02	0.02	0.01	0.02	0.02	0.01	2.72	2.55	5.78	0.59	0.37	0.52
K_2O	0.01	0.11	0.02	0.02	0.23	0.08	0.16	0.17	0.22	0.27	0.14	0.22	0.56	0.55	0.04	0.55	0.03	0.15	0.06	0.85	0.82	0.96	5.01	4.62	4.86
MgO	0.01	0.29	0.35	0.82	0.03	0.75	0.07	0.06	0.65	0.68	0.61	0.71	0.52	0.49	0.93	0.62	0.13	0.52	0.42	4.22	4.25	4.87	0.57	0.68	0.63
MnO	0.01	0.02	0.02	0.02	0.02	0.02	0.02	0.01	0.05	0.05	0.05	0.05	0.07	0.05	0.05	0.04	0.01	0.01	0.01	0.22	0.18	0.31	0.01	0.01	0.04
P_2O_5	0.01	0.03	0.06	0.01	0.03	0.05	0.06	0.04	0.02	0.04	0.03	0.06	0.03	0.32	0.15	0.03	0.06	0.14	0.12	0.47	0.45	0.48	0.08	0.08	0.09
LOI	0.01	7.02	8.01	9.26	8.45	10.23	7.56	9.23	10.11	9.81	10.33	10.01	9.86	10.02	10.55	11.02	8.95	42.41	39.87	1.54	1.11	1.52	5.14	5.26	5.42
Sum	–	99.52	99.56	99.50	99.78	99.78	99.73	99.57	99.82	99.82	99.68	99.77	99.77	99.73	99.76	99.84	99.54	99.63	99.68	99.89	99.79	99.96	99.91	99.67	99.83
Co (ppm)	0.2	53.7	111.0	57.0	47.5	62.2	18.3	18.3	12.2	10.2	11.7	15.5	14.1	15.1	11.9	12.4	19.6	12.1	11.4	39.7	40.7	37.5	10.1	16.1	16.0
Cr	1	869	678	761	633	603	644	588	235	217	187	166	167	209	307	142	739	13	13	108	110	89	121	130	121
Cs	0.1	0.4	0.3	0.2	0.7	0.3	0.5	0.6	0.5	0.5	0.4	0.4	0.6	0.7	0.4	0.5	0.2	0.2	0.1	0.5	0.4	0.6	7.7	7.5	8.2
Ga	0.05	43.7	48.3	56.2	54.1	48.7	40.0	51.2	29.2	29.7	36.0	34.6	29.3	31.6	44.8	25.7	45.2	1.0	0.5	19.1	20.6	22.5	27.3	25.7	28.7
Hf	0.02	2.68	3.73	4.14	4.51	4.94	3.31	3.95	9.61	8.82	8.23	8.34	8.36	8.64	6.78	9.02	4.14	0.21	0.26	3.11	2.14	4.08	2.44	2.68	2.58
Nb	0.5	84.7	93.2	96.5	95.7	104.0	93.9	94.1	79.0	70.1	65.5	69.2	99.3	76.7	126.0	72.9	130.0	1.4	2.9	13.2	12.8	17.5	17.1	17.2	18.6
Ni	1	271	233	121	243	123	202	156	33	33	36	32	35	41	7	26	66	5	6	75	64	41	33	46	51
Rb	0.1	0.7	0.1	0.1	3.0	0.8	2.1	2.9	4.2	4.1	1.8	2.8	12.0	9.9	0.6	9.4	0.1	0.2	0.8	11.5	9.8	8.7	190.0	177.0	200.0
Ba	0.2	26.9	46.0	8.3	38.8	52.4	31.7	21.7	95.9	126.0	93.6	128.0	172.0	152.0	37.8	230.0	32.3	12.7	8.1	320.1	260.2	345.6	524.0	769.0	564.0
Sr	0.1	51.6	64.7	40.9	66.9	91.1	31.7	70.2	30.6	36.0	31.4	41.6	52.8	87.1	76.2	43.4	126.0	1110.0	378	352.0	365.0	332.0	113.0	326.0	116.0
Ta	0.01	4.79	5.19	5.57	5.55	6.00	5.36	5.42	4.58	4.12	3.86	4.07	6.02	4.41	7.14	4.28	7.22	0.07	3.48	0.71	0.73	0.56	1.15	1.13	1.22
Th	0.02	7.6	11.4	8.7	11.4	12.5	13.9	13.0	16.9	14.1	10.8	13.5	17.9	16.4	13.3	11.7	16.0	0.7	0.3	1.5	1.6	2.9	14.4	14.3	14.7
U	0.02	11.0	8.5	9.5	9.2	8.7	8.0	7.6	20.4	18.2	16.3	16.4	9.0	16.2	8.5	18.8	10.2	0.8	3.1	0.5	0.4	0.8	1.9	2.0	2.0
V	1	1100	771	686	1070	751	761	628	396	388	343	362	378	417	503	307	772	8	41	245	240	244	182	178	192
Y	0.05	6.5	13.9	8.4	12.4	12.6	7.8	11.2	18.9	14.9	9.7	14.2	21.3	20.0	23.5	16.8	22.2	3.0	2.1	23.1	23.5	27.8	12.6	12.9	13.9
Zr	1	100	155	167	191	202	133	166	416	389	353	362	370	379	289	406	177	9	5	135	133	168	89	98	96
La (ppm)	0.5	10.20	24.60	4.43	11.60	23.70	16.40	20.00	6.96	5.19	4.07	7.83	64.10	14.10	65.20	9.18	47.70	2.76	2.56	14.50	17.60	21.70	43.00	42.00	44.60
Ce	0.5	44.20	96.20	34.00	63.90	150.00	63.00	86.60	18.30	13.50	11.40	21.10	103.00	64.90	168.00	24.00	256.00	5.97	5.47	32.80	33.30	47.50	86.00	84.70	90.10
Pr	0.05	2.99	5.17	1.57	3.97	5.07	3.84	5.39	1.34	1.01	0.85	1.48	9.75	3.19	17.40	1.64	9.74	0.58	0.57	4.64	4.65	6.24	9.44	9.14	9.60
Nd	0.5	10.20	19.30	6.93	18.30	19.50	12.90	19.10	4.42	3.40	2.83	4.74	27.00	11.70	67.50	5.19	36.80	2.21	2.19	18.84	18.70	24.40	34.30	33.10	35.60
Sm	0.02	2.19	3.88	1.65	6.33	4.06	2.64	4.27	0.92	0.71	0.59	0.90	3.57	2.47	15.80	0.97	8.53	0.46	0.46	5.01	4.71	6.51	6.06	5.66	6.29
Eu	0.01	1.23	1.56	0.43	1.62	1.06	1.23	1.77	0.24	0.18	0.15	0.23	0.87	0.62	3.78	0.24	2.64	0.11	0.09	1.64	1.75	2.06	0.96	0.87	1.06
Gd	0.05	1.98	3.57	1.47	4.86	3.68	2.58	3.68	1.52	1.11	0.88	1.33	5.18	2.48	13.70	1.43	8.22	0.51	0.41	4.89	5.03	6.19	3.92	3.83	4.40
Tb	0.01	0.40	0.65	0.35	0.89	0.59	0.46	0.66	0.44	0.34	0.26	0.36	0.59	0.53	1.99	0.41	1.22	0.08	0.07	0.82	0.77	0.91	0.41	0.43	0.46
Dy	0.02	2.41	4.15	2.41	4.52	3.59	2.84	4.07	3.20	2.53	1.91	2.58	3.86	3.64	9.24	2.98	6.51	0.47	0.39	4.91	4.91	5.68	2.48	2.54	2.65
Ho	0.02	0.45	0.80	0.50	0.74	0.66	0.53	0.75	0.76	0.61	0.45	0.61	0.81	0.81	1.44	0.70	1.11	0.10	0.08	0.92	0.92	1.16	0.50	0.54	0.54
Er	0.05	1.19	2.22	1.41	1.84	1.74	1.38	2.02	2.36	1.90	1.45	1.87	2.43	2.45	3.58	2.15	2.75	0.29	0.22	2.72	2.32	2.95	1.63	1.75	1.76
Tm	0.01	0.17	0.33	0.20	0.26	0.25	0.19	0.30	0.36	0.30	0.23	0.29	0.36	0.37	0.50	0.33	0.38	0.01	0.01	0.32	0.38	0.44	0.27	0.29	0.30
Yb	0.01	0.92	1.80	1.07	1.46	1.34	1.03	1.64	2.17	1.81	1.39	1.79	2.09	2.18	2.89	2.02	2.04	0.24	0.16	2.01	2.11	2.51	1.71	1.87	1.97
Lu	0.01	0.13	0.25	0.15	0.20	0.19	0.15	0.23	0.33	0.28	0.21	0.27	0.31	0.33	0.39	0.30	0.28	0.03	0.03	0.28	0.28	0.32	0.27	0.29	0.29

Bu-1 to Bu-16 are ores of the Kanirash bauxite deposit. Ls-1 and Ls-2 are the representative limestones of the Ruteh Formation. Samples from Sh-1 to Sh-3 are the representative shales of the Ruteh Formation. Samples from B-1 to B-3 are basalt rocks

DL detection limit, *LOI* loss on ignition, *RBO* red bauxite ore, *BRBO* brownish red bauxite ore, *DGCO* dark green bauxite ore

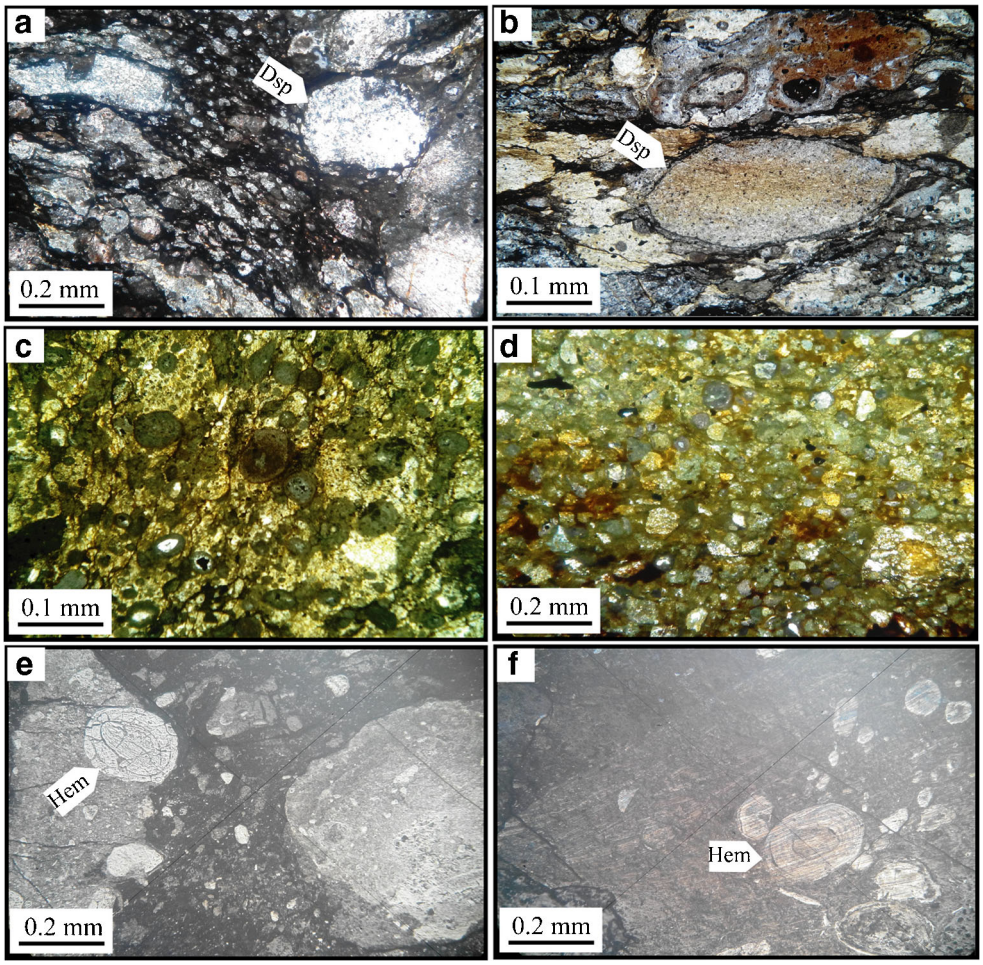

Fig. 4 Photomicrographs exhibiting textural and mineralogical aspects of the bauxite ores at Kanirash: **a** fluidal-collomorphic texture in the DGBO unit (cross-polarized light); **b** cataclastic texture in the DGBO unit (cross-polarized light); **c** ooidic texture in the DGBO unit (cross-polarized light); **d** distribution of spheroidal components in the DGBO unit (cross-polarized light); **e** allothigenic clasts with spherical to sub-rounded hematite clasts in the BRBO unit (reflected light); **f** pisoids with allothigenetic clasts in the RBO unit (reflected light). Dsp diaspore, Hem hematite

significant positive Ce anomalies, whereas the bauxite ores of the DGBO unit (samples from Bu-8 to Bu-16) are dominated by the downward-sloping patterns for LREE and relatively flat patterns for HREE with distinct negative Eu anomalies. REE patterns in the ores of the basal parts of the profile (RBO unit) are similar to those in the ores of the middle parts of the profile (BRBO unit). As shown in Fig. 7b, all of the bauxite units almost display a single pattern marked by the positive Ce and Eu anomalies, and the flat patterns of HREE. LREE in comparison with HREE have a broad range of variations in the representative ore samples of the Kanirash bauxite (Fig. 7a, b). The limestone in Fig. 7b display flat patterns for all of REE with exception of distinct negative Tm anomalies. HREE in comparison with LREE are depleted in the shale but are enriched in the basalt.

Discussion

Determination of origin of the bauxite through petrography

D'Argenio and Mindszenty (1995) believed that the mineralogical and chemical properties of ores in bauxite deposits mainly reflect environmental conditions. In the bauxite deposits, the presence of fluidal-collomorphic, ooidic, and pisoidic textures represent an autochthonous origin, whereas cataclastic texture, spheroidal components, and allothigenic clasts represent an allochthonous origin. Basically, the Kanirash bauxite formed initially "in situ" somewhere and later was reworked and re-deposited in the present location. The presence of sub-rounded ooids confirms this viewpoint. The fluidal-collomorphic texture is the result of dislocation of the primary colloids derived from weathering of the source rock during supergene and diagenetic processes (Bárdossy 1982).

Mineralogical characteristics of genetic significance

Diaspore is the main Al-hydroxide mineral in all of the bauxite units at Kanirash. Diaspore can form under the metamorphic, hydrothermal, and supergene environments (Bárdossy 1982; Gamaletsos et al. 2017; Ling et al. 2017). Diaspore in this study was formed in the reducing conditions of the depositional diagenetic/epigenetic environment (D'Argenio and Mindszenty 1995). The presence of sub-rounded diaspore grains may indicate that

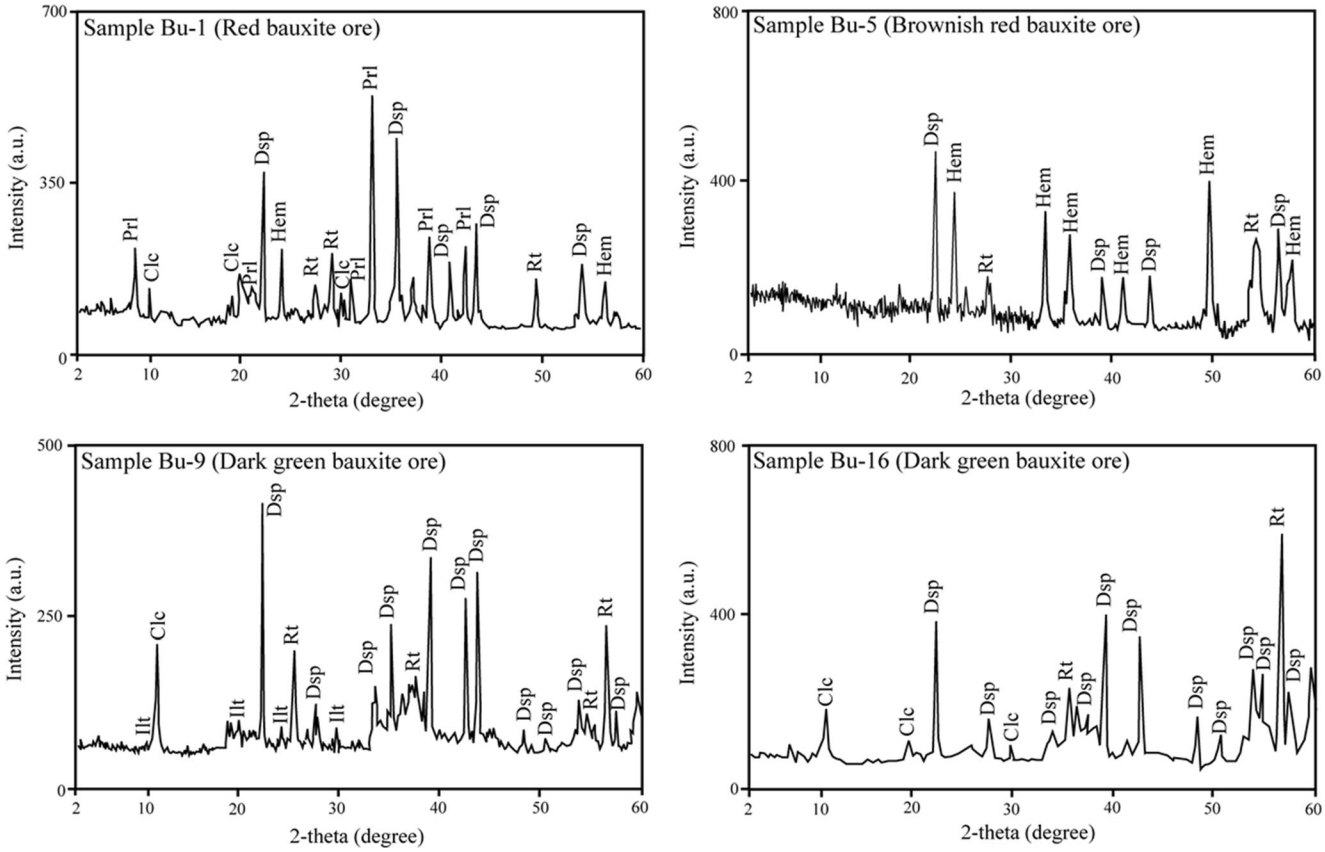

Fig. 5 Powder XRD diffractograms of the selective bauxite ores of the RBO, BRBO, and DRBO units from the Kanirash bauxite. Prl pyrophyllite, Hem hematite, Rt rutile, Dsp diaspore, Clc clinochlore, Ilt illite (taken from Whitney and Evans 2010)

transportation, to some extent, of the original ores occurred at Kanirash (Fig. 6d; Ling et al. 2015, and references therein). Hematite, as a major Fe-oxide mineral, in this study was generated by oxidation of Fe^{2+} ions released from the ferromagnesian silicates (e.g., biotite and hornblende) of the source rock (Nesbitt and Markovics 1997) which led to precipitation of Fe-hydroxides at near-neutral pH (Mongelli 2002, and references therein). Fe-rich coatings around concretions represent distribution and migration of iron and finally its precipitation (Monsels and Bergen 2017).

The role of decomposition of organic matters in generation of sulfide minerals both in metallic and non-metallic deposits, especially in the Pb-Zn metallogenic systems and bauxites was comprehensively discussed by several researchers (e.g., Kesler et al. 1994; Southgate et al. 2006; Laskou and Economou-Eliopoulos 2007; Ling et al. 2015). Organic matters are capable of absorbing a series of trace elements, including As, Sb, V, Mo, Ni, Re, Hg, S, Se, U, Cd, Ba, B, F, and W (Ling et al. 2015, and references therein). The presence of organic matters and sulfide minerals in the uppermost parts of the profile probably gave rise to generation of the acidic pore waters that percolated downward, as inferred from recent studies (e.g., Laskou and Economou-Eliopoulos 2007, 2013; Kalaitzidis et al. 2010; Ling et al. 2017). In turn, the presence of sulfide minerals in the upper parts of the profile can be related to the decomposition process of organic matters and the activities of micro-organisms. Decomposition process leads to release of a suite of anionic groups, including COO^{-}, NH_2, PO_4^{-}, S^{-}, HS^{-}, and SO_4^{2-} that are easily complexed with trace elements derived from the source rock (Ling et al. 2015). On the other hand, organic matters contain a considerable amounts of certain bivalent metal ions, such as Mn^{2+}, Cu^{2+}, Zn^{2+}, Fe^{2+}, and Mg^{2+} which play an important role in metabolic activities of microorganisms (Ling et al. 2015, and references therein). Decomposition of organic matters and Fe oxyhydroxides induced the formation of pyrite (Liu et al. 2010) that is an accessory mineral in the karst-type bauxite ores (Laskou and Economou-Eliopoulos 2007, 2013). In fact, pyrite was formed as the result of percolation of the surface solution into the karst interior depressions (D'Argenio and Mindszenty 1995). Sulfur could be procured either by decomposition of organic materials or by marine pore-waters during the course of transgression (D'Argenio and Mindszenty 1995).

The presence of diaspore, rutile, pyrophyllite, illite, clinochlore, and pyrite in the bauxite ores at Kanirash indicates a typical phreatic environment (reducing

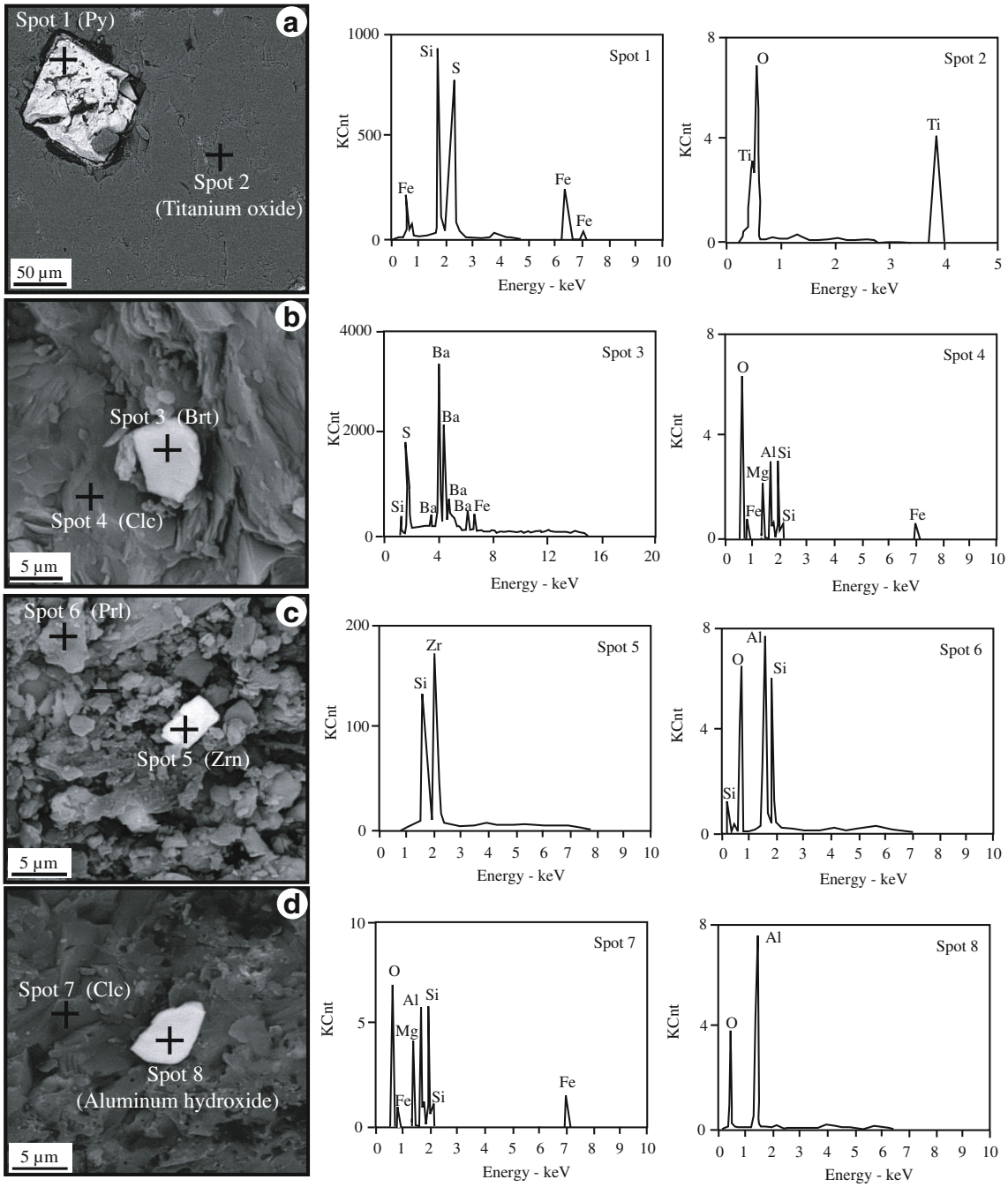

Fig. 6 SEM-EDS picture showing **a** pyrite in the matrix of rutile in the DGBO unit; **b**) barite in the clinochlore matrix in the DGBO unit; **c** zircon in the matrix of clinochlore in the DGBO unit; **d** diaspore in the matrix of pyrophyllite in the BRBO unit. Py pyrite, Clc clinochlore, Brt barite, Zrn zircon, Dsp diaspore, Rt rutile, Prl pyrophyllite (taken from Whitney and Evans 2010)

conditions), whereas the presence of hematite in the bauxite ores testifies to a typical vadose environment (oxidizing conditions). Based upon mineral assemblages, it suggests that the depositional diagenetic/epigenetic environment of the Kanirash bauxite was neither a vadose environment nor a phreatic one. Consequently, the Kanirash bauxite deposit was formed in a transitional zone between the vadose and the phreatic environments.

Behavior of major, minor, and trace elements

Major and minor elements

Bauxites are commonly formed by a successive sequence of processes. During the early stages of weathering processes, clay minerals (e.g., illite) are formed by breakdown of minerals susceptible to weathering, such as feldspars. Illite is altered to kaolinite when weathering progresses. Ultimately,

Table 3 Calculated elemental ratios and anomalies of Ce and Eu for the representative samples collected from bauxite ores, limestone, shale, and basalt

	Bu-1	Bu-2	Bu-3	Bu-4	Bu-5	Bu-6	Bu-7	Bu-8	Bu-9	Bu-10	Bu-11	Bu-12	Bu-13	Bu-14	Bu-15	Bu-16	Ls-1	Ls-2	B-1	B-2	B-3	Sh-1	Sh-2	Sh-3
ΣLREE (La-Eu) (ppm)	71.01	150.71	49.01	105.72	203.39	100.01	137.13	32.18	23.99	19.89	36.28	208.29	96.98	337.68	41.22	361.41	12.09	11.34	77.43	80.71	108.41	179.76	175.47	187.25
ΣHREE (Gd-Lu) (ppm)	7.65	13.77	7.56	14.77	12.04	9.16	13.35	11.14	8.88	6.78	9.10	15.63	12.79	33.73	10.32	22.51	1.73	1.37	16.87	16.72	20.16	11.19	11.54	12.37
ΣREE (La-Lu) (ppm)	78.66	164.48	56.57	120.49	215.43	109.17	150.48	43.32	32.87	26.67	45.38	223.92	109.77	371.41	51.54	383.92	13.82	12.71	94.30	97.43	128.57	190.95	187.01	199.62
La/Y	1.58	1.77	0.53	0.94	1.88	2.10	1.79	0.37	0.35	0.42	0.55	3.01	0.71	2.77	0.55	2.15	0.92	1.22	0.63	0.75	0.78	3.41	3.26	3.21
$(\Sigma LREE/\Sigma HREE)_N$	5.27	6.22	3.68	4.07	9.60	6.20	5.83	1.64	1.53	1.67	2.26	7.57	4.31	5.69	2.27	9.12	3.97	4.70	2.61	2.74	3.05	9.12	8.64	8.60
$(La/Yb)_N$	7.49	9.23	2.80	5.37	11.95	10.76	8.24	2.17	1.94	1.98	2.96	20.72	4.37	15.24	3.07	15.80	7.77	10.81	4.87	5.64	5.84	16.99	15.18	15.30
Eu/Eu*	1.75	1.24	0.82	0.87	0.81	1.40	1.32	0.60	0.60	0.62	0.62	0.60	0.74	0.76	0.60	0.94	0.67	0.61	0.98	1.07	0.96	0.58	0.55	0.60
Ce/Ce*	1.88	1.94	3.05	2.23	3.12	1.83	1.95	1.34	1.32	1.39	1.39	0.88	2.22	1.16	1.37	2.69	1.07	1.04	0.94	0.86	0.96	0.98	0.99	0.99

$(\Sigma LREE/\Sigma HREE)_N = (\Sigma LREE/\Sigma HREE)_{sample}/(\Sigma LREE/\Sigma HREE)_{chondrite}$, $(La/Yb)_N = (La/Yb)_{sample}/(La/Yb)_{chondrite}$, $Eu/Eu^* = Eu_N/\sqrt{(Sm_N \times Gd_N)^{0.5}}$, and $Ce/Ce^* = (2Ce_N)/(La_N + Pr_N)$. Abbreviations as in Table 2

kaolinite is decomposed to form insoluble Al-hydroxide (gibbsite) and soluble hydrated silica. During bauxitization process, mobile elements, such as alkali and alkali earth elements are leached out from the weathering profile through the breakdown of primary minerals of the aluminosilicate-rich parent rocks and move into solution. In general, behavior and distribution of trace elements in bauxite deposits are controlled by some parameters, including chemical composition of parent rocks, physicochemical conditions of ore-forming environment, chemical properties of elements, and diagenetic and epigenetic processes (Mordberg 1996; Meshram and Randive 2011). Calculations of mass change in bauxites have been accomplished in order to understand the behavior of major, minor, and trace elements during bauxitization process (Calagari and Abedini 2007; Abedini and Calagari 2013a). The percentage change of elements relative to the upper continental crust (UCC) with respect to Hf as a least mobile element is presented in Fig. 8.

Si, P, and K were leached throughout the profile, whereas Al and Ti show almost similar distribution patterns during weathering processes (see Fig. 8a). During the early stages of weathering, Si tends to be released from phyllosilicate crystal lattices and move into solution which in turn will modify the chemistry of weathering profile (e.g., Babechuk et al. 2014). Leaching of alkali and silica along with aluminum accumulation occurs under warm and humid conditions during bauxitization processes (Tardy 1992; Oliveira et al. 2013) that could be suggestive of a good drainage (Marker and Oliveira 1994). The intensive leaching and removal of Si, alkali, and alkali earth elements throughout the weathered profile is in full accordance with subtropical climate in Iran during late Permian (Muttoni et al. 2009, and references therein). Aluminum showed a limited variation along the entire studied profile (see Fig. 8a) suggesting that it behaved as a less mobile element during weathering processes, whereas Ti, due to a broad range in concentration variation along the profile at Kanirash, did not likely act as a less mobile element during bauxitization process (Fig. 8a). Fe and Ti were leached from the upper parts of the profile (DGBO unit) and subsequently re-deposited as hematite and rutile in the middle and basal parts of the profile (BRBO and RBO units; Fig. 8a). Ling et al. (2017) noted that high-grade bauxites (high content of Al_2O_3 and low content of SiO_2, Fe_2O_3, and TiO_2) tend to be formed under acidic conditions during bauxitization process. They also noted that acidic conditions and decomposition of organic matters are favorable for Fe mobility. Furthermore, pyrite oxidation brings about a decrease in soil pH and produces acidic condition in downward-percolating ground waters (Ling et al. 2017) facilitating the Fe removal from the upper parts of the weathered profile (Gamaletsos et al. 2017) and its concentration (as ferruginous phases) close to the subjacent carbonate bedrocks (Beyala et al. 2009; Ling et al. 2017, and references therein). Pyrite was identified by SEM-EDS examinations of the DGBO samples (see Fig. 6a).

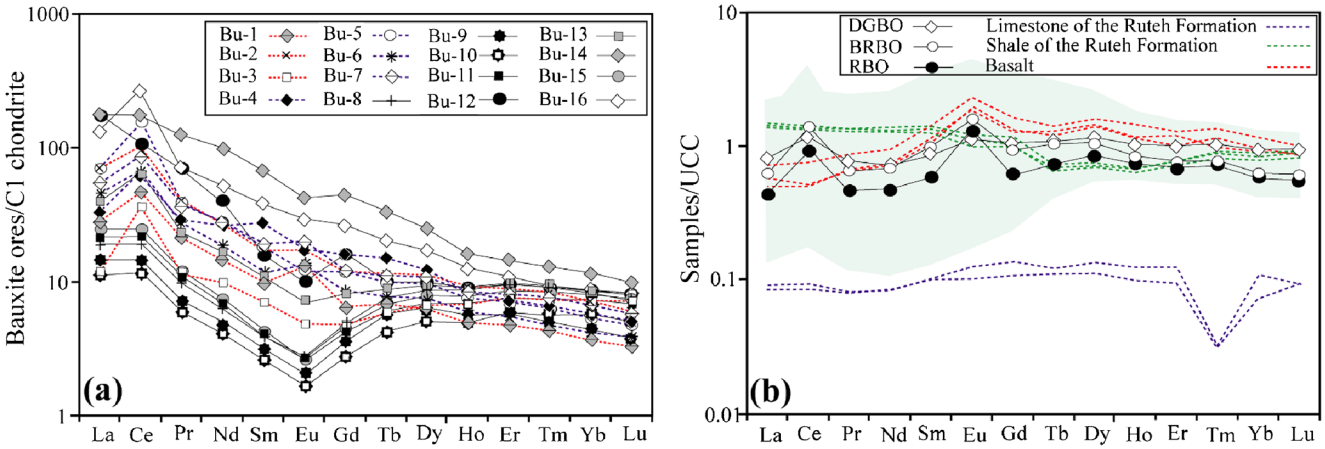

Fig. 7 **a** C1-chondrite-normalized REE spider patterns for the representative bauxite ore samples. **b** UCC-normalized REE spider patterns for the three bauxite units, basalt, shale, and limestone of the Ruteh Formation (see Fig. 3 for more information). Data for the chondrite and the UCC are from Taylor and McLennan (1985). The blue field represents the Kanirash bauxite ores

Trace elements

Large-ion lithophile elements (LILEs), such as Rb, Ba, Cs, and Sr in present case study were leached out completely along the entire weathered profile (see Fig. 8b). Among other LILE, Sr showed a wide range in concentration variation. Leaching of alkali and alkali earth elements represents breakdown of primary minerals (e.g., feldspars and 2:1 phyllosilicates) of the source rocks (Fernández-Caliani and Cantano 2010) and a good drainage (Beyala et al. 2009). Ga, Ta, and V showed a similar distribution pattern, regardless of the range of concentration changes. They were leached from the DGBO unit and subsequently concentrated in the BRBO and RBO units (see Fig. 8c). Among them, V displayed the highest concentration close to the underlying carbonate rocks of the Ruteh Formation. It suggests that Ga, Ta, V, and Ti that are commonly considered as immobile monitor elements during weathering processes, which did not act in such manner at Kanirash (Gamaletsos et al. 2017, and references therein). It seems that decomposition of organic matters and oxidation of pyrite promoted the removal and mobility of Ga, Ta, V, and Ti from the upper parts of the profile. The distribution patterns of Ga, Ta, and V mimic those of Ti and Fe. Enrichment of Ga, Ta, and V in the DGBO unit can be linked to hematite under

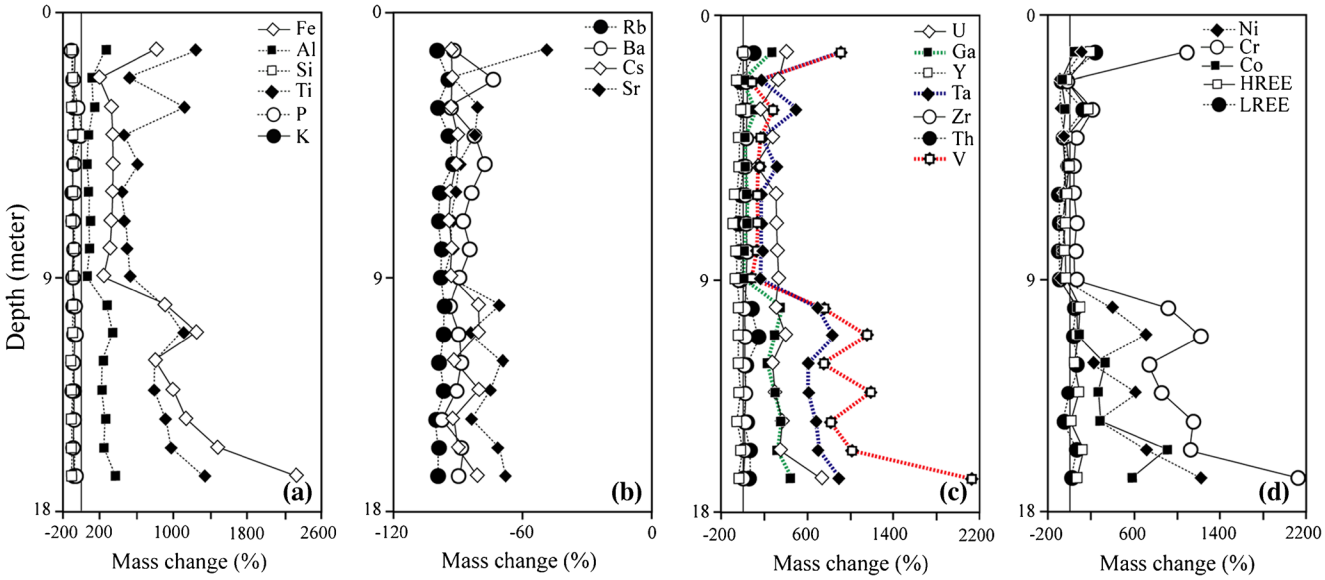

Fig. 8 Percentage change of chemical elements relative to the UCC with regard to Hf as a least mobile element, for **a** Fe, Al, Si, Ti, P, and K; **b** Rb, Ba, Cs, and Sr; **c** U, Ga, Y, Ta, Zr, Th, and V; and **d** Ni, Cr, Co, HREE, and LREE

sorption processes (Fernández-Caliani and Cantano 2010). U was enriched along the entire studied profile particularly in the parts of the profile which could be related to a reducing environment that was generated by the metal-reducing bacteria and/or the presence of humic acid, whereas significant enrichment of U in the lower parts is in accordance with adsorption onto hematite surfaces (Wei et al. 2014, and references therein). Th experienced slight enrichment as well as modest depletion. Zr and Y display negligible enrichment and depletion along the profile (see Fig. 8c), suggesting that they acted chiefly as immobile elements during chemical weathering.

Distribution pattern of Ni, Cr, and Co mimics that of Fe. They were leached from the upper parts of the profile and concentrated in the middle and basal parts (see Fig. 8d). Ni tends to be adsorbed by Fe oxyhydroxides during chemical weathering (Mongelli et al. 2014; Radusinović et al. 2017) but such behavior depends strongly on pH of the depositional environment (Sparks 1995). Hence, the presence of Fe-oxides in the BRBO and RBO units can be conceived as a main agent in Ni concentration in the basal parts of the studied profile at Kanirash (e.g., Laskou and Economou-Eliopoulos 2007). In addition, distribution of Cr and V along a weathered profile is mainly controlled by Fe oxyhydroxides (Marques et al. 2004). These elements tend to be easily substituted for Fe^{3+} in the crystal structure of Fe-oxyhydroxides (Schwertmann and Pfab 1996). As a result, concentration of Ni, Cr, and Co in the basal parts of the weathered profile at Kanirash was controlled by parameters, such as influence of the underlying carbonate rock as an efficient geochemical barrier and active buffer (Radusinović et al. 2017, and references therein), fluctuations of groundwater level, and adsorption onto hematite surfaces (Wei et al. 2014). Indeed, rising groundwater level and buffering nature of the carbonate bedrocks led to an increase in pH of the weathering solutions in the lowermost parts of the profile. LREE and HREE were leached from the DGBO unit and slightly concentrated in the BRBO and RBO units (see Fig. 8d). We suggest that some parameters, such as buffering nature of the underlying carbonate rock, fluctuations of groundwater level, and mineral control played important roles in REE concentration in the lower parts of the profile at Kanirash. Nevertheless, REE in the weathering systems tend to be re-deposited under neutral to alkaline pH conditions (Wang et al. 2010; Abedini et al. 2018).

According to Fig. 8 a, c, and d, distribution pattern of some major and trace elements with respect to Hf (as a least mobile element) suggests a change in the depositional environment of the bauxite ores with depth. The boundary between the DGBO unit and the BRBO unit (~ 9 m beneath the top of the bauxite horizon) can be regarded as a line separating the downward-percolating meteoric waters (or the ores related to the vadose environment) from the underground waters (or the ores related to the phreatic environment).

Fractionation of REE during bauxitization

The behavior of REE during weathering processes depends a great deal on Eh, pH, the role of microorganisms, mineral control, nature of the source rock, and accessory mineral association (Nesbitt 1979; McLennan 1989; Braun et al. 1990; Braun and Pagel 1994; Ma et al. 2007; Tang et al. 2009, 2013; Deng et al. 2014; Chen and Tang 2016). Distribution and geochemical behavior of REE during weathering provides some valuable insights into reconstruction of landscape evolution and the palaeo-evolution conditions (Marker and Oliveira 1994), redox conditions, and relationship between the weathered materials (e.g., Beyala et al. 2009). These will be testified by weathering intensity and drainage conditions (Marker and Oliveira 1994). Concentration and mobility of REE in the weathering profiles reflects geochemical and mineralogical composition of the parent rocks, duration of weathering, and palaeo-climatic and palaeo-hydrologic conditions (e.g., Radusinović et al. 2017).

The chondrite-normalized REE variation diagrams and ratios of $(\Sigma LREE/\Sigma HREE)_N$ and $(La/Yb)_N$ have long been taken as reliable indicators for fractionation of LREE from HREE in both metallic and non-metallic deposits, especially in bauxites (Mongelli et al. 2014; Khosravi et al. 2017). During weathering processes, mobility and concentration of REE may be controlled by Eh and pH of the depositional environment and geochemical behavior of REE. REE are mobile during pedogenesis processes (e.g., Maksimović and Pantó 1991), especially in humid and tropical climate conditions (Marker and Oliveira 1994). In this way, LREEs tend to be removed from the upper parts of the weathered profile under acidic conditions and to be concentrated in lower parts (Esmaeily et al. 2010; Mongelli et al. 2014). The broad range of LREE variations in the representative ore samples at Kanirash was likely attributed to substantial changes in pH of the ore-forming solutions (Fig. 7a, b). On the contrary, limited range of HREE in the bauxite ores indicates that HREE were likely incorporated in crystal lattices of the chemically-resistant accessory minerals. Additionally, the downward-percolating acidic waters played a crucial role in significant differentiation of LREE from HREE in the DGBO unit, whereas a weak differentiation of LREE from HREE was observed in the BRBO and RBO units adjacent to the carbonate bedrocks (Fig. 9a). Boundary between the BRBO unit and the DGBO unit can be regarded as the palaeo-level at which the downward-percolating acidic solutions encountered with groundwater table. High mobility of LREE relative to HREE is related to either difference in stability of REE-bearing accessory minerals against weathering (Boulange and Colin 1994; Nesbitt and Markovics 1997), acidic pH conditions, or moderate degree of bauxitization at Kanirash (Beyala et al. 2009).

There are numerous interpretations that could be attached to the observed $(\Sigma LREE/\Sigma HREE)_N$ variations. They might be inherited presumably from either the basalt or mobilization and fractionation of LREE and HREE at various weathering stages (from early to advanced) (Karadag et al. 2009), regardless of durability and intensity of weathering. Noticeable fractionation of LREE from HREE was not observed in the basal parts of the profile close to the carbonate bedrocks. It is likely related to the fixation of HREE in the chemically resistant accessory minerals. The pH of solutions during weathering is thought to be the key control on mobilization and fractionation of LREE from HREE (e.g., Nesbitt 1979; Boulange et al. 1990; Maksimović and Pantó 1991). Alkaline conditions are thought to promote adsorption of REE on secondary mineral surfaces, particularly enhancing the stability of the HREE complexes, and hence fractionating the LREE from the HREE (Muchangos 2006). The poor correlation between REE and ratios of $(\Sigma LREE/\Sigma HREE)_N$ and $(La/Yb)_N$ argues against a simple degree-of-weathering control on fractionation of REE. It implies instead significant changes in the pH of the weathering solutions during bauxitization along the profile. Buffering nature of the carbonate bedrocks and mineral control may have played important roles in REE distribution in the bauxite ores.

Ce and Eu anomalies in the bauxite ores

REE patterns can help to determine the presumptive source rock of bauxites, and the Ce and Eu anomalies may be applied to evaluate the physicochemical conditions during bauxitization (Mongelli 1997; Mameli et al. 2007; Karadag et al. 2009). Variations in the Ce and Eu anomalies are reflections of REE distribution in the weathered profiles (Condie et al. 1995). Previous studies have indicated anomalous behavior of cerium relative to its neighbors during weathering, due to the environmental conditions (e.g., Eh and pH), the presence of organic matters, and certain secondary mineral phases (Braun et al. 1990; Mongelli 1997; Wang et al. 2010). Ce is mobile at low pH (Braun et al. 1990; Hanilçi 2013) and reducing (Marker and Oliveira 1994) conditions. Variation of the Ce anomaly reflects weathering intensity and redox conditions being controlled by climate changes (Braun et al. 1998; Wei et al. 2014). Moreover, the Ce anomaly in the bauxite ores may be associated with weathering or stability of minerals, such as apatite, titanite, and zircon (Meshram and Randive 2011). The positive Ce anomaly is related to the incorporation of Ce^{4+} into the zircon crystal structure, due to the same oxidation state and similarity of Ce^{4+} ionic radius with Zr^{4+} (e.g., Boulange and Colin 1994; Meshram and Randive 2011). The range of ± 20% in Ce/Ce* does suggest differential mobility between cerium and other REE during weathering (Abedini and Calagari 2013a). The Ce anomaly yields an irregular manner, increasing downwards (from the upper parts of the profile) towards the basal parts (see Fig. 9b). According to Fig. 9b, the hematite-dominated bauxite ores (the RBO unit) are associated with high Ce anomalies, whereas the diaspore-dominated bauxite ores (the DGBO unit) are accompanied by low Ce anomalies. This may suggest that hematite in this case study played a fundamental role in concentration of cerium (e.g., Braun et al. 1990; Ohta and Kawabe 2001; Wei et al. 2014, and references therein). Compared to the middle and upper parts of the profile, the

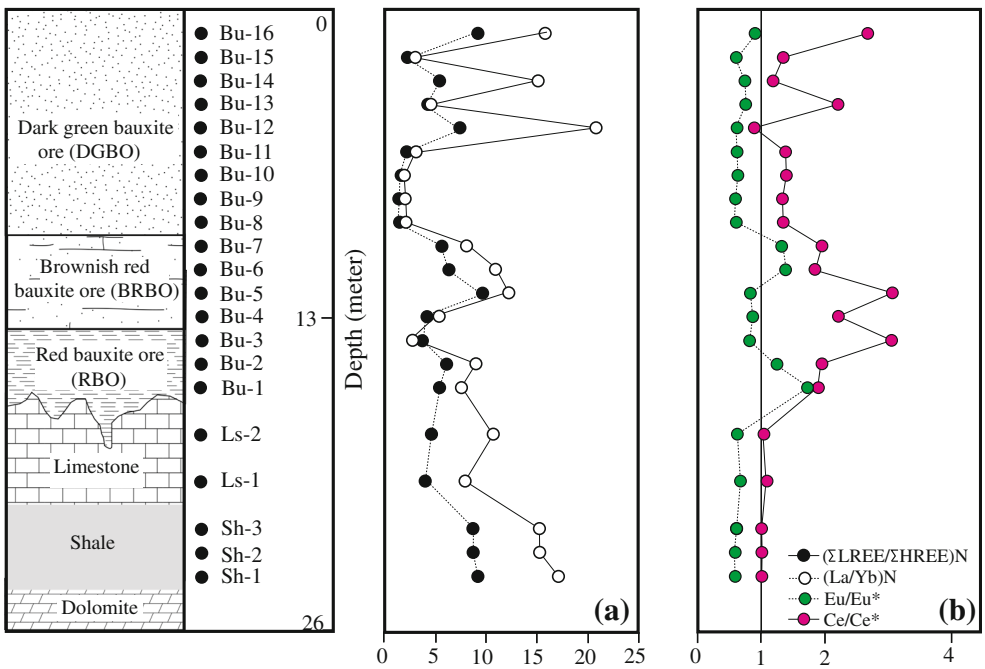

Fig. 9 Variations of geochemical indices along the studied profile at Kanirash. **a** $(\Sigma LREE/\Sigma HREE)_N$ and $(La/Yb)_N$. **b** Ce and Eu anomalies

positive Ce anomalies in the basal parts may be related to fluctuations of groundwater table and buffering nature of the carbonate bedrocks (Braun et al. 1990).

Variations of the Eu anomaly imply accumulation or decomposition of calcic plagioclase (Compton et al. 2003) and redox conditions (Wei et al. 2014). Negative Eu anomaly reflects reducing conditions of weathering environment and/or incorporation of Eu^{2+} into the plagioclase crystal structure. Variable breakdown of plagioclase or preferential leaching of Eu from the precursor rocks could generate the Eu anomalies during weathering (White et al. 2001). A relatively broad range of the Eu anomaly in the bauxite ores along the entire profile (see Fig. 9b) indicates that the Eu anomaly did not act as a proxy for provenance identification of the bauxite ores at Kanirash. The Eu anomaly shows a regular increase downwards from the upper parts of the profile towards basal parts. The increase in values of the Eu anomaly in the basal parts of the studied profile can be attributed to buffering nature of the carbonate bedrocks, fluctuations of groundwater table, and mineral control (Abedini and Calagari 2013c). Distribution pattern of the Eu anomaly along the entire profile mimics that of Fe, suggesting that behavior of the Eu anomaly was controlled by the same conditions governing the differential mobility and distribution of the latter.

Conclusions

(1) Based upon optical microscopic observations, the Kanirash bauxite deposit is allochthonous in origin.
(2) The presence of pyrite in the ores indicates that the depositional diagenetic/epigenetic environment was reducing in the uppermost parts of the profile.
(3) Distribution of trace elements, such as Ni, Cr, Co, U, V, Ga, and Ta along the weathered profile at Kanirash was mainly controlled by environmental conditions (Eh and pH) of soil and the activities of microorganisms.
(4) Concentration of Ni, Cr, and Co in the basal parts of the studied profile at Kanirash was controlled by buffering nature of the carbonate bedrocks, fluctuations of groundwater table, and certain host minerals.
(5) REE, especially the HREE, were likely hosted in crystal lattices of the chemically resistant accessory minerals (e.g., rutile), and the nature of ore-forming solutions played a fundamental role in differentiation of LREE from HREE at Kanirash.
(6) Boundary between the BRBO unit and the DGBO unit can be regarded as the palaeo-level at which the downward-percolating acidic solutions encountered with groundwater table. The depositional environment of the Kanirash bauxite deposit was neither a vadose environment nor a phreatic one. This deposit was formed in a transitional zone between the vadose and the phreatic environments.
(7) Distribution pattern of the Eu anomaly along the entire studied profile was controlled by the same environmental conditions governing the conduct of Fe distribution.

Acknowledgments Our gratitude is further expressed to Prof. Abdullah M. Al-Amri and associate editor for their advice, valuable suggestions, and editorial assistance, and also two anonymous reviewers for reviewing and making critical comments on this manuscript.

Funding information This work was financially fully supported by the Bureau of Deputy of Research and Complementary Education of Urmia University.

References

Abedini A, Calagari AA (2013a) Rare earth elements geochemistry of Sheikh-Marut laterite deposit, NW Mahabad, West-Azarbaidjan Province, Iran. Acta Geol Sin-Engl 87:176–185

Abedini A, Calagari AA (2013b) Geochemical characteristics of Kanigorgeh ferruginous bauxite horizon, West-Azarbaidjan Province. NW Iran Period Miner 82:1–23

Abedini A, Calagari AA (2013c) Geochemical characteristics of bauxites: the Permian Shahindezh horizon, NW Iran. Neues Jahrb Geol Palaontol Abh 270:301–324

Abedini A, Calagari AA (2014) REE geochemical characteristics of titanium-rich bauxites: the Permian Kanigorgeh horizon, NW Iran. Turk J Earth Sci 23:513–532

Abedini A, Calagari AA (2015) Rare earth element geochemistry of the Upper Permian limestone: the Kanigorgeh mining district, NW Iran. Turk J Earth Sci 24:1–18

Abedini A, Calagari AA (2017) Geochemistry of claystones of the Ruteh Formation, NW Iran: implications for provenance, source-area weathering, and paleo-redox conditions. Neues Jahrb Miner Abh 194:107–123

Abedini A, Calagari AA, Rezaei Azizi M (2018) The tetrad-effect in rare earth elements distribution patterns of titanium-rich bauxites: evidence from the Kanigorgeh deposit, NW Iran. J Geochem Explor 186:129–142

Abedini A, Khosravi M, Calagari AA (2019a) Geochemical characteristics of the Arbanos karst-type bauxite deposit, NW Iran: implications for parental affinity and factors controlling the distribution of elements. J Geochem Explor 200:249–265

Abedini A, Rezaei Azizi M, Calagari AA (2019b) REE mobility and tetrad effects in bauxites: an example from the Kanisheeteh deposit, NW Iran. Acta Geodyn Geomater 193:11–26

Babechuk MG, Widdowson M, Kamber BS (2014) Quantifying chemical weathering intensity and trace element release from two contrasting basalt profiles, Deccan Traps, India. Chem Geol 363:56–75

Bárdossy G (1982) Karst bauxites. Bauxite deposits on carbonate rocks. Dev Econ Geol 14 pp. 441. Elsevier, Amsterdam

Bárdossy G, Aleva GJJ (1990) Lateritic bauxites. Dev Econ Geol 27 pp. 624. Elsevier, Amsterdam

Beyala VKK, Onana VL, Priso ENE, Parisot JC, Ekodeck GE (2009) Behaviour of REE and mass balance calculations in a lateritic profile over chlorite schists in South Cameroon. Chem Erde-Geochem 69: 61–73

Boni M, Rollinson G, Mondillo N, Balassone G, Santoro L (2013) Quantitative mineralogical characterization of karst bauxite deposits in the Southern Apennines, Italy. Econ Geol 108:813–833

Boulange B, Colin F (1994) Rare earth element mobility during conversion of nepheline syenite into lateritic bauxite at Passa Quatro, Minais Gerais, Brazil. Appl Geochem 9:701–711

Boulange B, Muller JP, Sigolo JB (1990) Behaviour of the rare earth elements in a lateritic bauxite from syenite (Bresil). Chem Geol 84:350–351

Braun JJ, Pagel M (1994) Geochemical and mineralogical behavior of REE, Th and U in the Akongo lateritic profile (SW Cameroon). Catena 21:173–177

Braun JJ, Pagel M, Muller JP, Bilong P, Michard A, Guillet B (1990) Ce anomalies in lateritic profiles. Geochim Cosmochim Acta 54:781–795

Braun JJ, Viers J, Dupré B, Polve M, Ndam J, Muller JP (1998) Solid/liquid REE fractionation in the lateritic system of Goyoum, East Cameroon: the implication for the present dynamics of the soil covers of the humid tropical regions. Geochim Cosmochim Acta 62:273–299

Calagari AA, Abedini A (2007) Geochemical investigations on Permo-Triassic bauxite horizon at Kanisheeteh, east of Bukan, West-Azarbaidjan, Iran. J Geochem Explor 94:1–18

Chen YJ, Tang HS (2016) The great oxidation event and its records in North China Craton. In: Zhai MG, Zhao Y, Zhao TP (eds) Main tectonic events and metallogeny of the North China Craton, Springer, Singapore, pp 281–304

Compton SJ, White AR, Smith M (2003) Rare earth element behavior in soils and salt pan sediments of a semi-arid granitic terrain in the Western Cape, South Africa. Chem Geol 201:239–255

Condie KC, Dengate J, Cullers RJ (1995) Behavior of rare earth elements in a paleoweathering profile on granodiorite in the Front Range, Colorado, USA. Geochim Cosmochim Acta 59:279–294

D'Argenio B, Mindszenty A (1995) Bauxites and related paleokarst: tectonic and climatic event markers at regional unconformities. Eclogae Geol Helv 88:453–499

Deng XH, Chen YJ, Yao JM, Bagas L, Tang HS (2014) Fluorite REE-Y (REY) geochemistry of the ca. 850 Ma Tumen molybdenite-fluorite deposit, eastern Qinling, China: constraints on ore genesis. Ore Geol Rev 63:532–543

Duzgoren-Aydin NS, Aydin A, Malpas J (2002) Distribution of clay minerals along a weathered pyroclastic rock profile, Hong Kong. Catena 50:17–41

Esmaeily D, Rahimpour-Bonab H, Esna-Ashari A, Kananian A (2010) Petrography and geochemistry of the Jajarm Karst bauxite ore deposit, NE Iran: implications for source rock material and ore genesis. Turk J Earth Sci 19:267–284

Fernández-Caliani JC, Cantano M (2010) Intensive kaolinization during a lateritic weathering event in South-West Spain: mineralogical and geochemical inferences from a relict paleosol. Catena 80:23–33

Gamaletsos PN, Godelitsas A, Kasama T, Church NS, Douvalis AP, Göttlicher J, Steininger R, Boubnov A, Pontikes Y, Tzamos E, Bakas T, Filippidis A (2017) Nano-mineralogy and -geochemistry of high-grade diasporic karst-type bauxite from Parnassos-Ghiona mines, Greece. Ore Geol Rev 84:228–244

Hanilçi N (2013) Geological and geochemical evolution of the Bolkardagi bauxite deposits, Karaman, Turkey: transformation from shale to bauxite. J Geochem Explor 133:118–137

Kalaitzidis S, Siavalas G, Skarpelis N, Araujo CV, Christanis K (2010) Late Cretaceous coal overlying karstic bauxite deposits in the Parnassus-Ghiona Unit, Central Greece: coal characteristics and depositional environment. Int J Coal Geol 81:211–226

Kamineni DC, Efthekharnezad J (1977) Mineralogy of the Permian laterite of northwestern Iran. Tschermaks Mineral Petrogr Mitt 24: 195–204

Karadag MM, Küpeli S, Arýk F, Ayhan A, Zedef V, Döyen A (2009) Rare earth element (REE) geochemistry and genetic implications of the Mortaş bauxite deposit (Seydişehir/Konya-Southern Turkey). Chem Erde-Geochem 69:143–159

Kesler SE, Jones HD, Furman FC, Sassen R, Anderson WH, Kyle JR (1994) Role of crude oil in the genesis of Mississippi Valley-type deposits: evidence from the Cincinnatirch. Geol 22:609–612

Khosravi M, Abedini A, Alipour S, Mongelli G (2017) The Darzi-Vali bauxite deposit, West-Azarbaidjan Province, Iran: critical metals distribution and parental affinities. J Afr Earth Sci 129:960–972

Laskou M, Economou-Eliopoulos M (2007) The role of micro-organisms on the mineralogical and geochemical characteristics of the Parnassos-Ghiona bauxite deposits, Greece. J Geochem Explor 93: 67–77

Laskou M, Economou-Eliopoulos M (2013) Bio-mineralization and potential biogeochemical processes in bauxite deposits: genetic and ore quality significance. Mineral Petrol 107:471–486

Ling KY, Zhu XQ, Wang ZG, Han T, Tang HS, Chen WY (2013) Metallogenic model of bauxite in Central Guizhou Province: an example of Lindai deposit. Acta Geol Sin-Engl 87(6):1630–1642

Ling KY, Zhu XQ, Tang HS, Wang ZG, Yan HW, Han T, Chen WY (2015) Mineralogical characteristics of the karstic bauxite deposits in the Xiuwen ore belt, Central Guizhou Province, Southwest China. Ore Geol Rev 65:84–96

Ling KY, Zhu XQ, Tang HS, Li SX (2017) Importance of hydrogeological conditions during formation of the karstic bauxite deposits, Central Guizhou Province, Southwest China: a case study at Lindai deposit. Ore Geol Rev 82:198–216

Ling KY, Zhu XQ, Tang HS, Du SJ, Gu J (2018) Geology and geochemistry of the Xiaoshanba bauxite deposit, Central Guizhou Province, SW China: implications for the behavior of trace and rare earth elements. J Geochem Explor 190:170–186

Liu X, Wang Q, Deng J, Zhang Q, Sun S, Meng J (2010) Mineralogical and geochemical investigations of the Dajia Salento-type bauxite deposits, western Guangxi, China. J Geochem Explor 105:137–152

Lopez JMG, Bauluz B, Fernández-Nieto C, Oliete AY (2005) Factors controlling the trace element distribution in fine-grained rocks: the Albian kaolinite-rich deposits of the Oliete Basin (NE Spain). Chem Geol 214:1–19

Ma J, Wei G, Xu Y, Long W, Sun W (2007) Mobilization and redistribution of major and trace elements during extreme weathering of basalt in Hainan Island, South China. Geochim Cosmochim Acta 71:3223–3237

MacLean WH, Bonavia FF, Sanna G (1997) Argillite debris converted to bauxite during karst weathering: evidence from immobile element geochemistry at the Olmedo deposit, Sardinia. Mineral Deposita 32: 607–616

Maksimović Z, Pantó G (1991) Contribution to the geochemistry of the rare earth elements in the karst-bauxite deposits of Yugoslavia and Greece. Geoderma 51:93–109

Mameli P, Mongelli G, Oggiano G, Dinelli E (2007) Geological, geochemical and mineralogical features of some bauxite deposits from Nurra (Western Sardinia, Italy): insights on conditions of formation and parental affinity. Int J Earth Sci 96:887–902

Marker A, Oliveira JJ (1994) Climatic and morphological control of rare earth element distribution in weathering mantles on alkaline rocks. Catena 21:179–193

Marques JJ, Schulze DG, Curi N, Mertzman SA (2004) Trace element geochemistry in Brazilian Cerrado soils. Geoderma 121:31–43

McLennan SM (1989) Rare earth elements in sedimentary rocks: influence of provenance and sedimentary processes. Geochem Miner Rare Earth Elem:169–200

Meshram RR, Randive KR (2011) Geochemical study of laterites of the Jamnagar district, Gujarat, India: implications on parent rock, mineralogy and tectonics. J Asian Earth Sci 42:1271–1287

Mongelli G (1997) Ce-anomalies in the textural components of Upper Cretaceous karst bauxites from the Apulian carbonate platform (southern Italy). Chem Geol 140:69–79

Mongelli G (2002) Growth of hematite and boehmite in concretions from ancient karst bauxite: clue for past climate. Catena 50:43–51

Mongelli G, Boni M, Buccione R, Sinisi R (2014) Geochemistry of the Apulian karst bauxites (southern Italy): chemical fractionation and parental affinities. Ore Geol Rev 63:9–21

Monsels DA, Bergen MJ (2017) Bauxite formation on Proterozoic bedrock of Suriname. J Geochem Explor 180:71–90

Mordberg LE (1996) Geochemistry of trace elements in Paleozoic bauxite profiles in northern Russia. J Geochem Explor 57:187–199

Muchangos AC (2006) The mobility of rare earth and other elements in the process of alteration of rhyolitic rocks to bentonite (Lebombo Volcanic Mountainous Chain, Mozambique). J Geochem Explor 88: 300–303

Muttoni G, Gaetani M, Kent DV, Sciunnach D, Angiolini L, Berra F, Garzanti E, Mattei M, Zanchi A (2009) Opening of the Neo-Tethys Ocean and the Pangea B to Pangea a transformation during the Permian. GeoArabia 14:17–48

Nesbitt HW (1979) Mobility and fractionation of rare earth elements during weathering of a granodiorite. Nature 279:206–210

Nesbitt HW, Markovics G (1997) Weathering of granodiorite crust, long-term storage of elements in weathering profiles, and petrogenesis of siliclastic sediments. Geochim Cosmochim Acta 61:1653–1670

Ohta A, Kawabe I (2001) REE(III) adsorption onto Mn dioxide (δ-MnO_2) and Fe oxyhydroxide: Ce(III) oxidation by δ-MnO_2. Geochim Cosmochim Acta 65:695–703

Oliveira FS, Varajão AFDC, Varajão CAC, Boulangé B, Soares CCV (2013) Mineralogical, micromorphological and geochemical evolution of the facies from the bauxite deposit of Barro Alto, Central Brazil. Catena 105:29–39

Radusinović S, Jelenković R, Pačevski A, Simić V, Božović D, Holclajtner-Antunović I, Životić D (2017) Content and mode of occurrences of rare earth elements in the Zagrad karstic bauxite deposit (Nikšić area, Montenegro). Ore Geol Rev 80:406–428

Schwertmann U, Pfab G (1996) Structural V and Cr in lateritic iron oxides: genetic implications. Geochim Cosmochim Acta 60:4279–4283

Southgate PN, Kyser TK, Scott DL, Large RR, Golding SD, Polito PA (2006) A basin system and fluid-flow analysis of the Zn-Pb-Ag Mount Isa-type deposits of northern Australia: identifying metal source, basinal brine reservoirs, times of fluid expulsion, and organic matter reactions. Econ Geol 101:1103–1115

Sparks DL (1995) Environmental soil chemistry. Academic Press, New York

Tang HS, Chen YJ, Wu G, Yang T (2009) Rare earth element geochemistry of carbonates of Dashiqiao Formation, Liaohe Group, eastern Liaoning province: implications for Lomagundi Event. Acta Petrol Sin-Engl 25:3075–3093

Tang HS, Chen YJ, Santosh M, Zhong H, Yang T (2013) REE geochemistry of carbonates from the Guanmenshan Formation, Liaohe Group, NE Sino-Korean Craton: Implications for seawater compositional change during the Great Oxidation Event. Precambrian Res 227:316–336

Tardy Y (1992) Diversity and terminology of lateritic profiles. In: Martini IP, Chesworth W (eds) Weathering, soils & paleosols. Elsevier, Amsterdam, pp 379–406

Tardy Y, Kobilsek B, Paquet H (1991) Mineralogical composition and geographical distribution of African and Brazilian periatlantic laterites. The influence of continental drift and tropical paleoclimates during the past 150 million years and implications for India and Australia. J Afr Earth Sci 12:283–295

Taylor SR, McLennan SM (1985) The continental crust: its composition and evolution. Blackwell, Oxford

Wang Q, Deng J, Liu X, Zhang Q, Sun S, Jiang C, Zhou F (2010) Discovery of the REE minerals and its geological significance in the Quyang bauxite deposit, West Guangxi. China J Asian Earth Sci 39:701–712

Wang QF, Liu XF, Yan CH, Cai SH, Li ZM, Wang YR, Zhao JM, Li GJ (2012) Mineralogical and geochemical studies of boron-rich bauxite ore deposits in the Songqi region, SW Henan, China. Ore Geol Rev 48:258–270

Wei X, Ji H, Wang S, Chu H, Song C (2014) The formation of representative lateritic weathering covers in south-central Guangxi (southern China). Catena 118:55–72

White AF, Bullen TD, Schulz MS, Blum AE, Huntington TG, Peters NE (2001) Differential rates of feldspar weathering in granitic regoliths. Geochim Cosmochim Acta 65:847–869

Whitney DL, Evans BW (2010) Abbreviations for names of rock-forming minerals. Am Mineral 95:185–187